doi:10.1038/nature11656

Supplementary Tables

Table S1. Average single-cell carbon assimilation and doubling times determined from ^{13}C-incubations.

	AT% ^{13}C excess[#]		C-fixation per cell[#] (amol C day^{-1})		% CO_2-derived C[§]	Doubling time[#] (days)
incubation	$^{13}CH_4$	$^{13}CO_2$	$^{13}CH_4$	$^{13}CO_2$		$^{13}CO_2$
ANME-2	0.22 ± 0.009* (n = 198)	0.51 ± 0.02 (n = 155)	0.39 ± 0.02* (n = 198)	9.9 ± 0.33 (n = 155)	96*	130 ± 24 (n = 155)
DSS	0.18 ± 0.006* (n = 133)	0.40 ± 0.01 (n = 210)	0.11 ± 0.004* (n = 133)	2.6 ± 0.07 (n = 210)	96*	160 ± 28 (n = 210)

[#] Mean ± SE
[§] Calculated from the cellular C-fixation rates obtained for $^{13}CH_4$ and $^{13}CO_2$ incubations.
* Methane-derived carbon could either come from direct CH_4 assimilation or assimilation of inorganic carbon produced during AOM.

Note that the at% ^{13}C excess for bulk biomass in the $^{13}CH_4$ incubation was 0.17 and thus comparable to the average cellular at% ^{13}C excess obtained by nanoSIMS.

Table S2. Free energies of reactions at physiological standard state (pH=7) and under *in vitro* conditions for reactions involving the disproportionation of zerovalent sulfur.

Eqn.	Reaction	$\Delta G^{\circ\prime}_{rxn}$ kJ rxn^{-1}	ΔG_{rxn} kJ rxn^{-1}	Ratio HS^-:SO_4^{2-}
a	$4S + 4H_2O \rightarrow 5H^+ + SO_4^{2-} + 3HS^-$	40.8	-48.7	3
b	$\frac{1}{2}S_{8(aq)} + 4H_2O \rightarrow 5H^+ + SO_4^{2-} + 3HS^-$	243.1	–49.4	3
c	$4HS_2^- + 4H_2O \rightarrow SO_4^{2-} + 7HS^- + 5H^+$	8.2	–49	7
d	$4S_2^- + 4H_2O \rightarrow H^+ + SO_4^{2-} + 7HS^-$	–60.9	–46.7	7
e	$2S_3^{2-} + 4H_2O \rightarrow 3H^+ + SO_4^{2-} + 5HS^-$	1.2	–54.1	5
f	$\frac{4}{3}S_4^{2-} + 4H_2O \rightarrow \frac{11}{3}H^+ + SO_4^{2-} + \frac{13}{3}HS^-$	20.2	–52.1	4.33
g	$S_5^{2-} + 4H_2O \rightarrow 4H^+ + SO_4^{2-} + 4HS^-$	26.7	–51.0	4
h	$\frac{4}{5}S_6^{2-} + 4H_2O \rightarrow \frac{21}{5}H^+ + SO_4^{2-} + \frac{19}{5}HS^-$	28.4	–50.4	3.8
i	$\frac{4}{6}S_7^{2-} + 4H_2O \rightarrow \frac{26}{6}H^+ + SO_4^{2-} + \frac{22}{6}HS^-$	28.3	–50.2	3.67
j	$\frac{4}{7}S_8^{2-} + 4H_2O \rightarrow \frac{31}{7}H^+ + SO_4^{2-} + \frac{25}{7}HS^-$	27.7	–50.4	3.57

Activity coefficients for the elemental sulfur are assumed to approach 1. The concentration of dissolved cyclooctasulfur ($S_{8(aq)}$) and the G°_f were obtained from ref. 69. Concentrations of polysulfides were calculated using a spreadsheet provided by A. Kamyshny, using the values from ref. 49 and assuming that the polysulfide system is saturated with respect to elemental sulfur. The stoichiometric ratio of sulfide to sulfate is also provided for each disproportionation reaction.

Table S3. Concentrations, calculated activities, and free energies of formation of the elements used in thermodynamic calculations.

Component	Added Concentration M	Calculated Free Ion Conc. M	Calculated Activity Coefficient	Calculated Activity M	$\Delta G°_f$ kJ mol^{-1}
$CH_{4\ (aq)}$	1.5×10^{-3}	1.5×10^{-3}	1.16	1.74×10^{-3}	**–34.39**
SO_4^{2-}	2.76×10^{-2}	1.59×10^{-2}	0.169	2.71×10^{-3}	**–744.6**
HCO_3^-	3.0×10^{-2}	2.06×10^{-2}	0.690	1.14×10^{-2}	**–586.8**
HS^-	5×10^{-4} as total $H_2S_{(diss)}$	3.7×10^{-4}	0.651	2.0×10^{-4}	**12.05**
HS_2^-		1.46×10^{-5}	0.651	9.5×10^{-6}	**20.2**
H^+ pH=7				3.16×10^{-8}	**0**
H_2O			0.982	0.982	**–237.18**

Table S4. Free energies of reactions (rxn) at standard state and under *in vitro* conditions for reactions considered in the text.

Equation	Reaction	$\Delta G°_{rxn}$ kJ rxn^{-1}	ΔG_{rxn} kJ rxn^{-1}
1	$CH_{4(aq)} + SO_4^{2-} \rightarrow HS^- + HCO_3^- + H_2O$	–33	–34
2	$7CH_{4(aq)} + 8SO_4^{2-} + 5H^+ \rightarrow 4HS_2^- + 7HCO_3^- + 11H_2O$	–438	–186
3	$4HS_2^- + 4H_2O \rightarrow SO_4^{2-} + 7HS^- + 5H^+$	208	–51

Table S5. Free energies of reactions at physiological standard state (pH=7) and under *in vitro* conditions for reactions involving the oxidation of methane to elemental sulfur, and the oxidation of methane via elemental sulfur reduction.

Eqn.	Reaction	$\Delta G^{\circ\prime}_{rxn}$ kJ rxn^{-1}	ΔG_{rxn} kJ rxn^{-1}
k	$CH_{4(aq)} + \frac{8}{6}SO_4^{2-} + \frac{10}{6}H^+ \rightarrow \frac{8}{6}S^0 + \frac{14}{6}H_2O + HCO_3^-$	–46.5	–19.7
l	$CH_{4(aq)} + \frac{8}{6}SO_4^{2-} + \frac{10}{6}H^+ \rightarrow \frac{1}{6}S_{8(aq)} + \frac{14}{6}H_2O + HCO_3^-$	–39.3	–19.5
m	$CH_{4(aq)} + 4S^0 + 3H_2O + \rightarrow 5H^+ + 4HS^- + HCO_3^-$	7.7	–84.1
n	$CH_{4(aq)} + \frac{4}{8}S_{8(aq)} + 3H_2O + \rightarrow 5H^+ + 4HS^- + HCO_3^-$	–13.8	84.7

Activity coefficients for the elemental sulfur are assumed to approach 1. The concentration of dissolved cyclooctasulfur ($S_{8(aq)}$) and the ΔG°_f for $S_{8(aq)}$ were obtained from ref. 69.

Supplementary Discussion

The concept of zerovalent sulfur as an intermediate

Solid rhombohedral elemental sulfur, colloidal elemental sulfur, and polysulfides (S_n^{2-} and their protonated forms with n=2-9) contain sulfur in oxidation state 0. These zerovalent sulfur (S^0) containing compounds differ with regard to their chemical properties, such as solubility and reactivity. Rhombic cyclooctasulfur (S_8) is only sparingly soluble (ca. 50 nM in seawater at 25°C)[67], but colloidal sulfur can be produced in many different forms that are quite soluble and remain in solution for long periods of time (see also ref. 74). In its polysulfide form, S^0 is also soluble[49,68]. Polysulfides can be formed chemically, mainly as a result of a fast (seconds to minutes) equilibrium reaction between elemental sulfur and dissolved sufide. The concentrations of chemically formed polysulfides and polysulfide-zerovalent sulfur increase proportionally to the concentrations of total dissolved sulfide as long as there is a source of elemental sulfur to "dissolve". In a sulfidic saturated elemental sulfur solution, approximately 9% of the total dissolved sufide will be associated with polysulfides of various chain lengths. For instance, at pH 7 and 500 µM total dissolved sulfide, 47 µM of sulfide will exist in polysulfides. This polysulfide component will carry with it 142 µM zerovalent sulfur, of which 15 µM will be dissolved disulfide. The polysulfide chain length distribution under these conditions is mainly controlled by sulfide concentration and pH. At ph 7-8, the most abundant polysulfides are S_n=2, 4, 5 and 6. Their respective concentrations in our incubation can be estimated based on polysulfide equilibrium calculations.

Our data indicate that ANME reduce sulfate to S^0. Whether this sulfur leaks out of the cell or is actively secreted is not known. The ANME may actually continue to reduce the S^0 formed upon sulfate reduction to sulfide; the thermodynamics of this reaction is favorable (see Table S5). Yet, part of the S^0 becomes available as free polysulfides, which can be disproportionated by the DSS bacteria. HPLC measurements of freshly inoculated cultures revealed that up to 600 µM polysulfide S^0 is present in the biomass, while detectable but very low amounts of free polysulfide were present in the overlying fresh medium (Supplementary Fig. 1). The medium from an old culture that was exposed to *ca.* 20 mmol l^{-1} sulfide also contained large amounts of polysulfides, which were most likely released from the AOM biomass.

Under sulfidic conditions polysulfide zerovalent sulfur disproportionation is energetically more favorable than elemental sulfur disproportionation (Table S2), and the size of the polysulfide chain does not matter when we consider equilibrium distributions

of polysulfide sulfur under *in vitro* conditions. Our conclusion, that it is the disulfide (of all polysulfides) that is disproportionated, is based on the uniquely high stoichiometric ratio of produced HS^-:SO_4^{2-} during our experiments.

At circumneutral pH, protonated disulfide (HS_2^-) is thought to be the most abundant polysulfide. The small molecular size of HS_2^- may additionally contribute to its preferential uptake by the bacteria. Moreover, disulfide complexes are common in living cells (e.g. cysteine-cystin and glutathione-glutathine disulfides) and are routinely handled by enzymes. Unfortunately, there is currently no method available for direct measurements of environmentally significant amounts of dissolved disulfide. The methyl trifluoromethanesulfonate method (which is based on methylation of terminal S groups) can only accurately detect polysulfides with chain lengths between three and eight[68].

The ANME or the DSS, per se, cannot directly control the distribution of polysulfides in solution because of the rapid chemical equilibration reactions. If, for instance, the S_2^{2-} is taken up by the DSS, the spectrum of polysulfide compounds will rapidly adjust to re-establish the equilibrium S_2^{2-} concentration, somewhat analogous to acid-base equilibrium (as long as the system is saturated with elemental sulfur and pH is not changing). Also, sulfide production during disulfide disproportionation will lead to an increase in the total sulfide concentration and a corresponding increase in the concentration of S_2^{2-}.

Our sulfur addition experiment shows that the DSS can also utilize externally-supplied polysulfides. Hence they might not necessarily associate with the ANME if other sources of zerovalent sulfur are present. Moreover, our *in vitro* results and the observations of single living ANME-2 cells in the environment suggest that ANME might not depend on the DSS either. Therefore, the ANME-DSS co-existence does not represent a true example of obligate syntrophy.

^{35}S-sulfide labeling experiment

Although the usual potential electron acceptors for sulfide oxidation (oxygen, nitrate/nitrite, reduced iron/manganese) were absent in our anaerobic culture, sulfate reduction coupled to sulfide oxidation (a so-called comproportionation) can in theory serve as a source of S^0 (e.g. disulfide; Eq. 4).

$$SO_4^{2-} + 7HS^- + H^+ \rightarrow 4S_2^{2-} + 4H_2O \quad (4)$$

We tested comproportionation as a potential source of biomass-bound S^0 by incubating the Isis culture in the presence of $H^{35}S^-$. The stoichiometry of comproportionation

dictates that the formed S^0 will be to 7/8 sulfide-derived and to 1/8 sulfate-derived (Eq. 4). Hence, ^{35}S should accumulate ~7 times faster in the biomass in the incubations with $H^{35}S^-$ than with $^{35}SO_4^{2-}$. However, the rate of ^{35}S accumulation in the biomass was substantially slower with $H^{35}S^-$ than with $^{35}SO_4^{2-}$ and the ^{35}S-enrichment was only transient (Supplementary Fig. 7; note that the ^{35}S-label in the biomass disappears already after 1 hour). This is in contrast to the continuous increase in ^{35}S content of the biomass observed in the incubations with ^{35}S-labeled sulfate (Supplementary Fig. 5). We therefore conclude that comproportionation is not a source of intracellular sulfur. Considering the fast isotopic equilibration of sulfur and sulfide[75], it is likely that the initial ^{35}S-enrichment at 1 hour is a result of fast isotope exchange of sulfide in the medium with the extracellular sulfur in the AOM aggregates. Moreover, these results indicate that there is little to no ^{35}S exchange between $H^{35}S^-$ in the medium and the intracellular sulfur.

Supplementary Figures

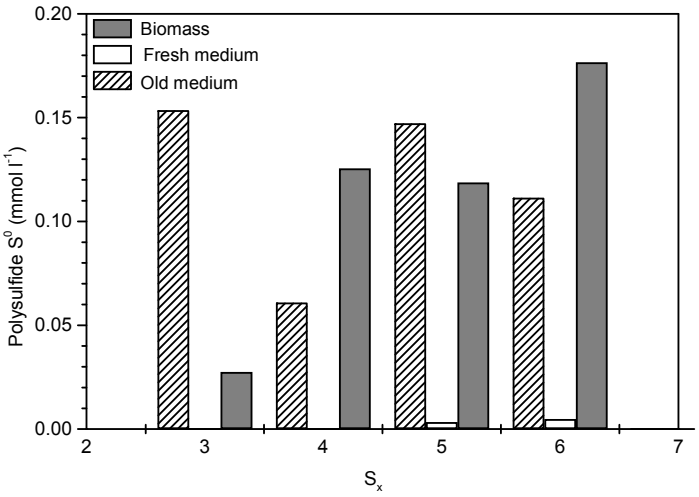

Supplementary Figure 1. Distribution of individual polysulfides (S_x) in biomass, and old (*ca.* 20 days) and fresh (*ca.* 3 days) medium from the Isis culture, as detected by HPLC.

Total polysulfide zerovalent sulfur (i.e. sum of total zerovalent sulfur in all detectable polysulfides) was calculated to be 0.008 mmol l^{-1} in the fresh medium and 0.34 mmol l^{-1} in the old medium. Based on the polysulfide concentrations, the measured polysulfide-zerovalent sulfur in the biomass represents ~ 4 mmol $g_{dry\ weight}^{-1}$ or ~ 10 wt %.

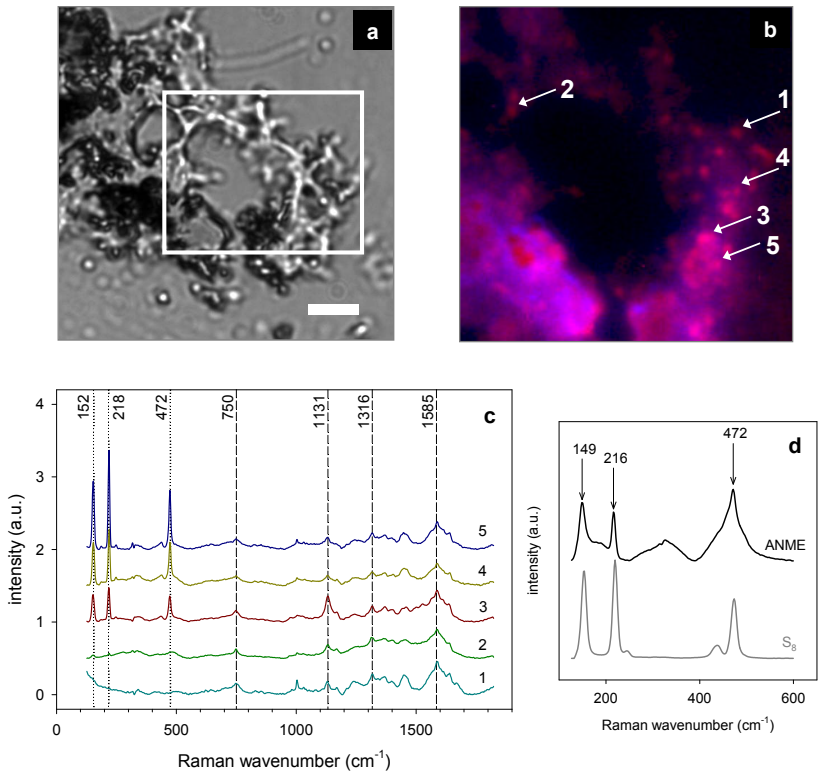

Supplementary Figure 2. Raman analyses of Isis enrichment culture.

a. Bright field image of Isis enrichment culture. Inset shows area corresponding to the fluorescence image in **b**. Scale bar is 10 µm. **b.** Fluorescence image of Isis culture stained with FISH (probe Arch915, in red) and observed without embedding under the Raman epifluorescence microscope. Blue shows autofluorescence of the biological material in the aggregate. Arrows indicate cells, from which Raman spectra in **c** were recorded. **c.** Raman spectra of selected ANME-2 cells (1-5) with characteristic peaks for S_8 (152, 218, 472 cm^{-1}; dotted line) and cytochrome *c* (750, 1131, 1316, 1585 cm^{-1}; short-dashed line). Note that not all ANME-2 cells contain sulfur, which agrees well with the lower $^{32}S/^{12}C$ ratio of some ANME-2 cells as determined by nanoSIMS. Although we do not expect to see polysulfides under the conditions used for Raman imaging, it should be noted that disulfides and other polysulfides would have other Raman peaks than S_8 (ref. 22) only the peak around 474 cm^{-1} is shared. **d.** Average (n=8) Raman spectrum of untreated, unlabeled ANME-2 cells recorded in anaerobic solution. Note the presence of peaks characteristic for S_8. Elemental sulfur standard is shown for comparison.

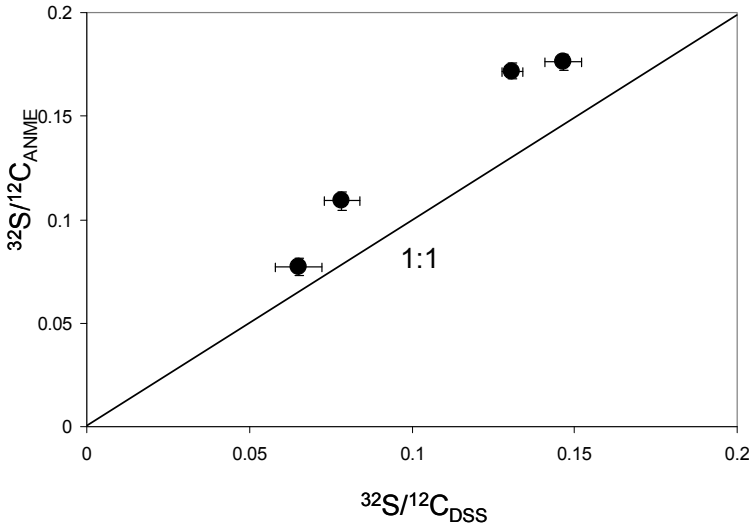

Supplementary Figure 3. Average relative sulfur content of ANME-2 ($^{32}S/^{12}C_{ANME}$) *vs.* DSS ($^{32}S/^{12}C_{DSS}$).

Four different thin sections from two Isis aggregates were investigated. Each contained on average 100 cells. Note that the $^{32}S/^{12}C$ ratio is always significantly higher (i.e. above 1:1 line) for ANME than for the DSS from a given field of view. Error bars represent standard error of mean.

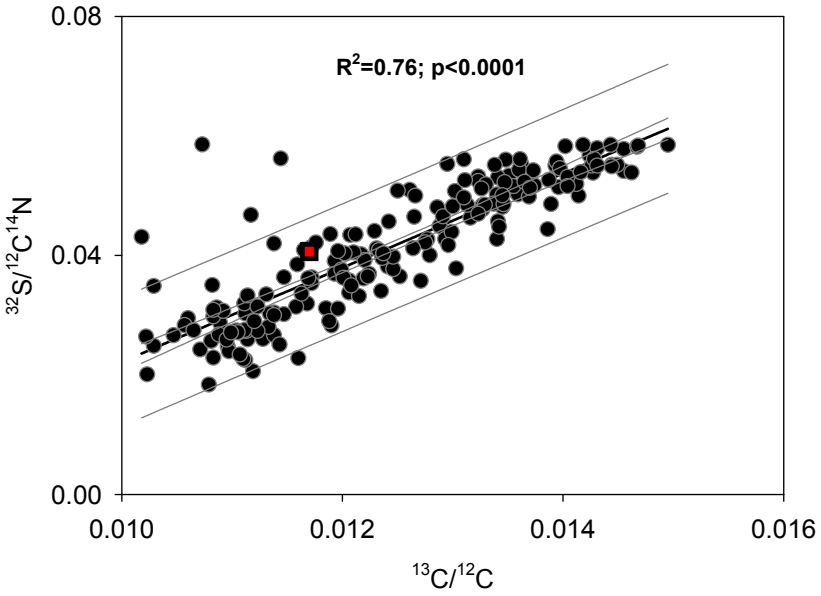

Supplementary Figure 4. The $^{13}C/^{12}C$ *vs.* $^{32}S/^{12}C^{14}N$ relationship determined from $^{13}CH_4$ incubations for ANME cells.

As shown in Fig. 2f, a significant correlation exists between the $^{13}C/^{12}C$ and $^{32}S/^{12}C$ ratio for ANME cells (n = 198) indicating that ANME turn over sulfur proportionally to methane assimilation (methane oxidation). Correlation for the ANME cells is maintained also when $^{32}S/^{12}C^{14}N$ ratio is used instead of $^{32}S/^{12}C$ (n=194). Red square indicates average for DSS cells.

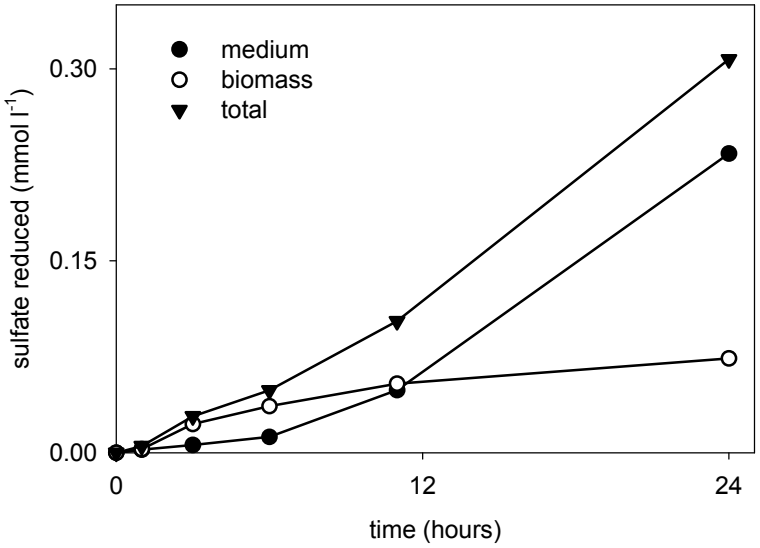

Supplementary Figure 5. Sulfate reduction in the Isis enrichment culture.

Time-dependent accumulation of total reduced sulfate, reduced sulfur in medium, and reduced sulfur in biomass for the Isis enrichment culture incubated in the presence of $^{35}SO_4^{2-}$.

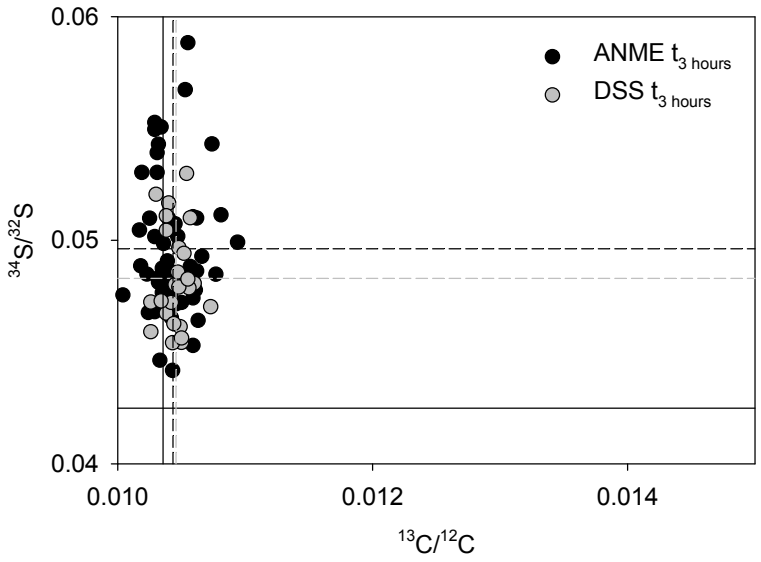

Supplementary Figure 6. Dissolved inorganic carbon and sulfate-derived sulfur uptake by ANME and DSS cells.

$^{34}S/^{32}S$ *versus* $^{13}C/^{12}C$ ratio for ANME (n > 70) and DSS (n > 20) cells incubated with $^{34}SO_4^{2-}$ and $^{13}CO_2$ as determined by nanoSIMS. Axes are scaled to represent a 500 ‰ enrichment in the respective isotope. Full lines represent natural abundance of ^{13}C and ^{34}S, as determined from t_0 sample analysis. Dotted lines represent average $^{13}C/^{12}C$ and $^{34}S/^{32}S$ values for ANME and DSS after 3 hours of incubation under AOM conditions.

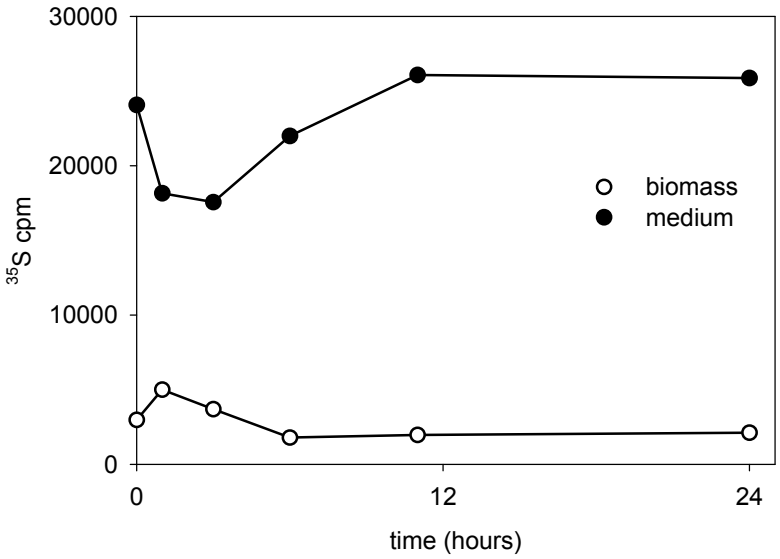

Supplementary Figure 7. ^{35}S accumulation in the biomass and in the medium in the Isis enrichment culture incubated with sulfate and methane in the presence of ^{35}S-sulfide (also see Suppl. Discussion)**.**

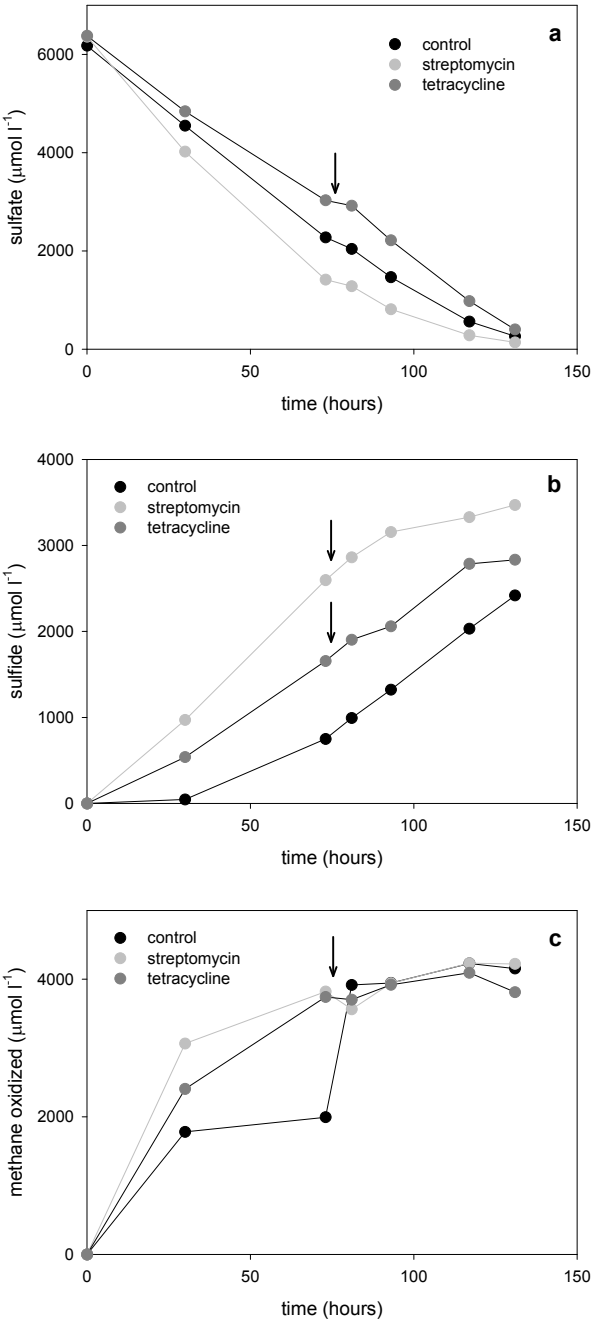

Supplementary Figure 8. Sulfate (a), sulfide (b) and CH_4 oxidation (c) during the course of the antibiotics experiment. Arrows indicate the addition of tetracycline or streptomycin, respectively.

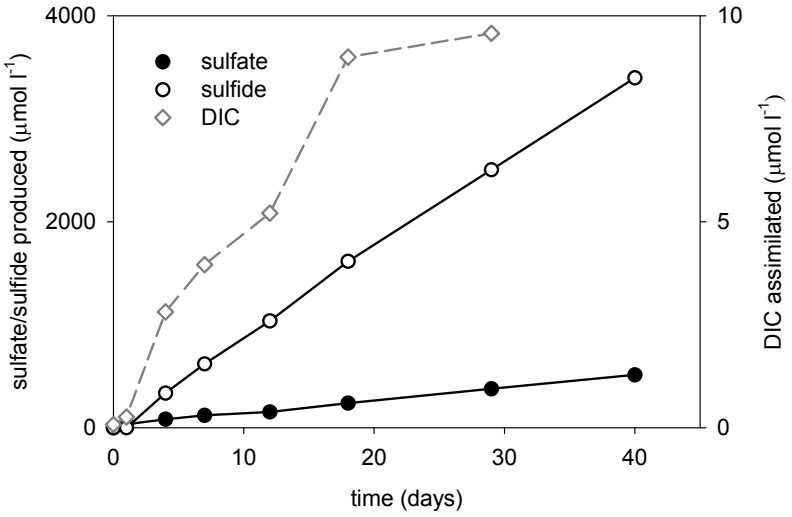

Supplementary Figure 9. Dissolved inorganic carbon (DIC) assimilation and sulfate and sulfide production in the Isis enrichment culture incubated with colloidal sulfur and ^{14}C-DIC in the absence of methane.

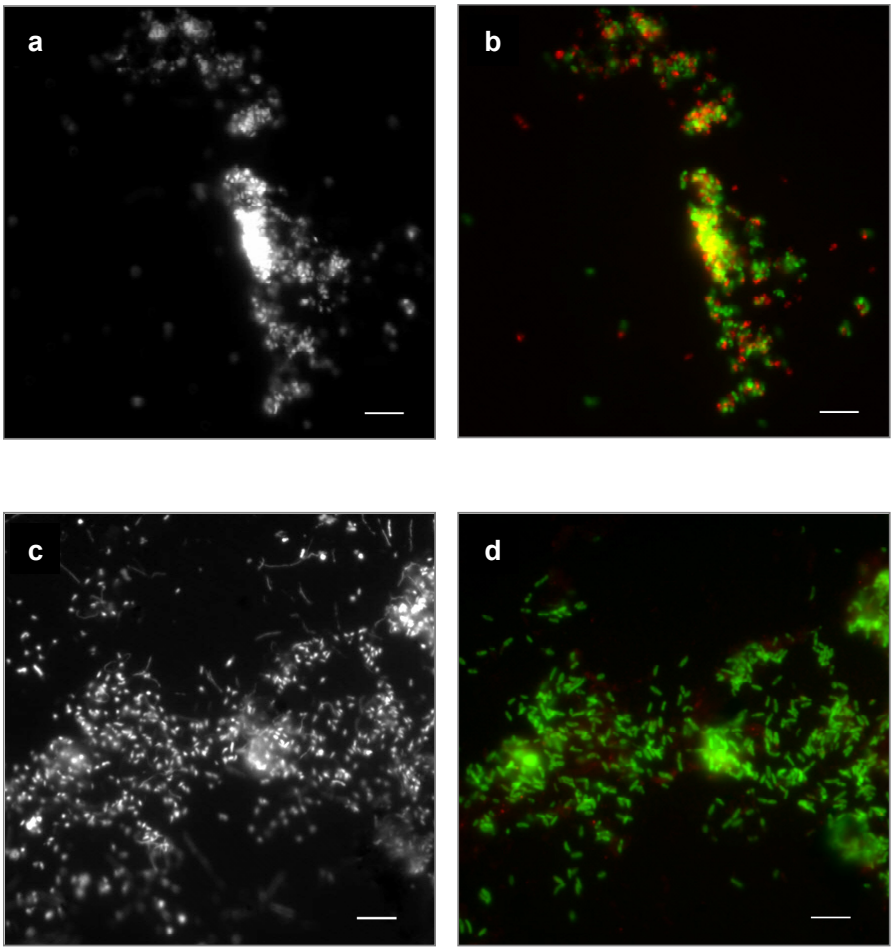

Supplementary Figure 10. CARD-FISH image of Isis enrichment culture grown under AOM (a, b) and disproportionating (c, d) conditions. a. DAPI image of the Isis culture before the addition of colloidal sulfur. **b.** corresponding fluorescence image where ANME-2 (red) and DSS (green) were stained by specific probes (ANME-2-538 and DSS-658, respectively). **c.** DAPI image of the Isis culture after 270 days of incubation without methane with colloidal sulfur. **d.** corresponding fluorescence image with ANME-2- (red) and DSS- (green) specific probes. ANME-2 were not detected in this incubation.

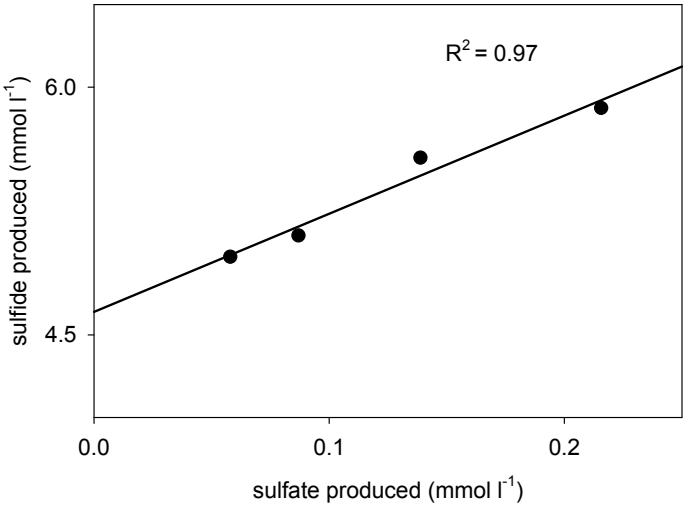

Supplementary Figure 11. Sulfate *vs.* sulfide production in the Isis enrichment culture incubated with sulfate and methane in the presence of ^{35}S-sulfide.

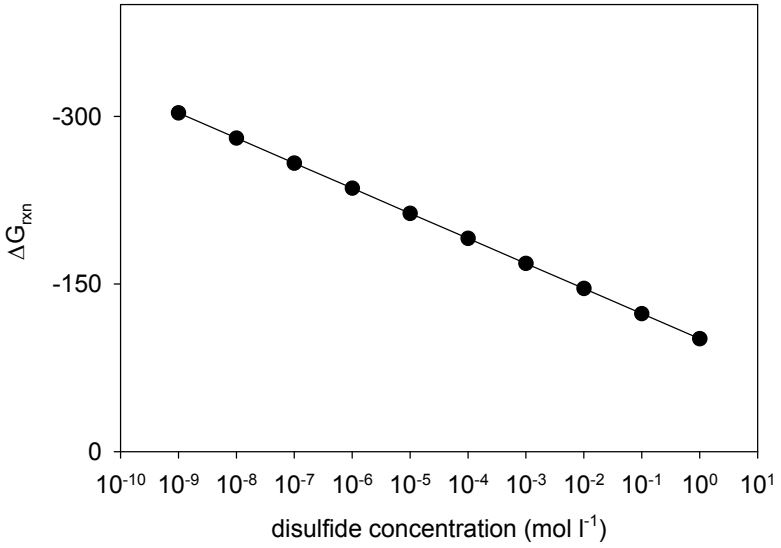

Supplementary Figure 12. Effect of disulfide concentration on the free energy gain of methane oxidation coupled to the reduction of sulfate to disulfide (ΔG_{rxn}).
With decreasing disulfide concentration energy gain of the methane-oxidizing archaea producing disulfide increases. X axis is in logarithmic scale.

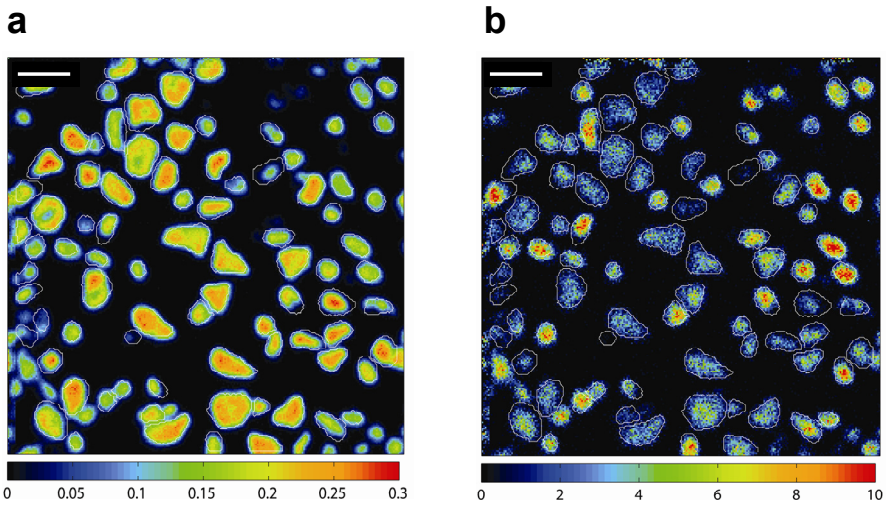

Supplementary Figure 13. The individual $^{32}S/^{12}C$ (a) and $^{31}P/^{12}C$ (b) ratios used to generate the composite image in Fig 2c. Scale bar is 2 μm.

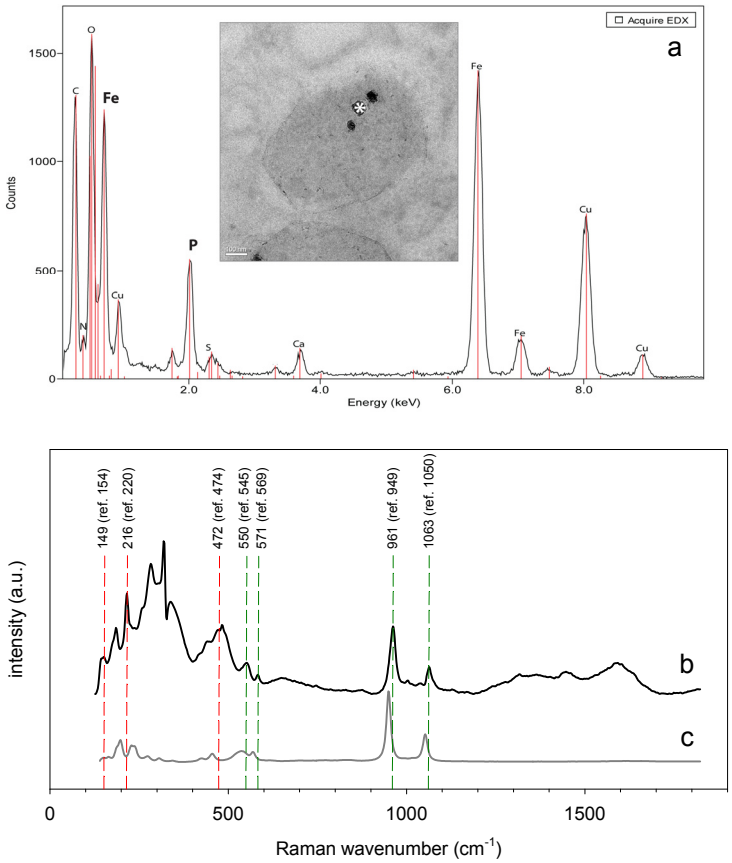

Supplementary Figure 14. TEM, EDX and Raman evidence for the presence of iron- and phosphate- rich particles in the DSS cells in AOM aggregates.

a. TEM image (inset) of bacteria from AOM culture which contain conspicuous intracellular particles. EDX analysis of the particle (indicated by an asterisk) shows strong enrichment in Fe and P. Copper signal originates from copper TEM grids. Scale bar is 100 nm. **b.** Average spectrum of fixed and sectioned DSS-type cells (n=3) with prominent peaks at 550, 571, 961 and 1063 cm^{-1} (green dashed lines) attributed to $Fe_3(PO_4)_2$ and peaks at 149, 216 and 472 cm^{-1} (red dashed lines) characteristic for elemental sulfur. **c.** Average spectrum of vivianite [$Fe_3(PO_4)_2$ from Bolivia], which is shown for comparison. For all signature peaks the published values of the respective reference compounds are indicated in brackets (ref. 21 and 22 [S_8], ref. 76 [vivianite]). The CaF_2 peak (originating from the supporting CaF_2 glass) was removed from the DSS spectra to increase clarity.

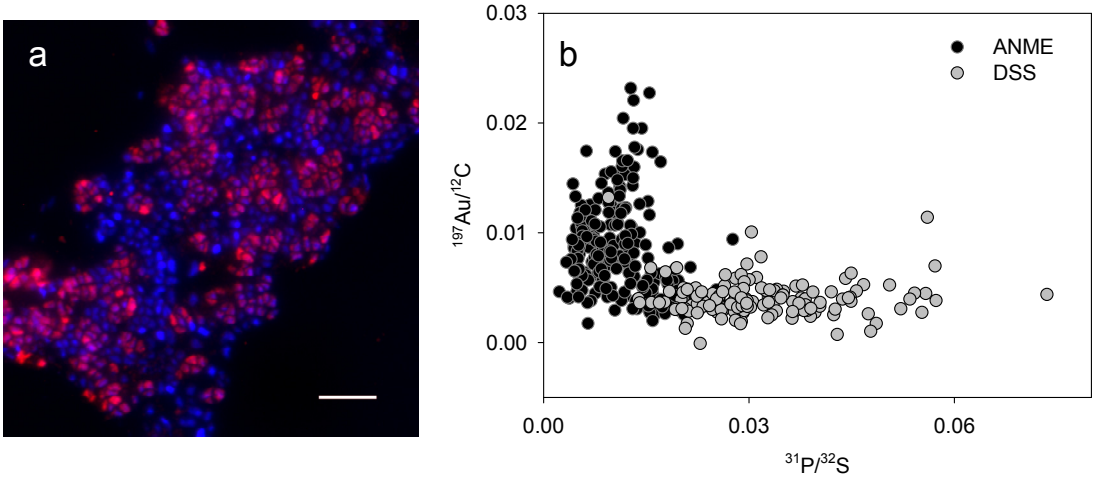

Supplementary Figure 15. Validation of the immuno-fluorescent/-gold anti-Mcr-labeling for nanoSIMS.

a. Fluorescent image of a microbial aggregate stained with secondary antibodies labeled with both FITC and nanoGold. ANME in red (FITC signal was changed to red during image processing), DAPI signal in blue. Scale bar is 5 µm. **b.** A plot representing ANME (n=242) and DSS (n=140) cells from 5 different fields of view (3 different Isis aggregates). Note that only ANME show substantial enrichment in ^{197}Au (originating from Au-labeled antibodies).

Supplementary References

74. Kamyshny, A. & Ferdelman, T. G. Dynamics of zero-valent sulfur species including polysulfides at seep sites on intertidal sand flats (Wadden Sea, North Sea). *Mar. Chem.* **121**: 17-26 (2010).
75. Fossing, H. & Jørgensen, B. B. Isotope exchange reactions with radiolabeled sulfur compounds in anoxic seawater. *Biogeochemistry* **9**: 223-245 (1990).
76. Frost, R. L., Martens, W., Williams, P. A. & Kloprogge, J. T. Raman and infrared spectroscopic study of the vivianite-group phosphates vivianite, baricite and bobierrite. *Mineral. Mag.* **66**: 1063-1073 (2002).